Emergency Management
Science and Technology

ARTICLE

Open Access

https://doi.org/10.48130/emst-0025-0021
Emergency Management Science and Technology **2025**, 5: e023

Assessment of the performance of a novel T-Stub-enhanced ConXL moment connection under fire

Chanachai Thongchom[1,2], Ali Ghamari[3*], Alejandro Jiménez Rios[4] and Imran Karimi[5]

[1] *Department of Civil Engineering, Faculty of Engineering, Thammasat School of Engineering, Thammasat University, Pathumthani 12120, Thailand*
[2] *Thammasat University Research Unit in Structural Foundation and Engineering, Department of Civil Engineering, Pathumthani 12120, Thailand*
[3] *Department of Civil Engineering, Il.C., Islamic Azad University, Ilam, Iran*
[4] *Department of Architecture & Civil Engineering, University of Bath, Bath, United Kingdom*
[5] *Department of Civil Engineering, Tabriz University, Tabriz, Iran*
* Corresponding author, E-mail: ali.ghamari@iau.ac.ir, aghamari@alumni.iust.ac.ir

Abstract

Box columns are widely recognized for their satisfactory performance in structural applications; however, their complex fabrication, particularly with the use of continuity plates, remains a significant drawback. The ConXtech® ConXL™ (referred to as ConXL) moment connection addresses this limitation, offering advantages such as improved industrialization processes and construction quality. This study proposes an innovative enhancement to the ConXL connection by incorporating a T-stub for application with unfilled box columns. The enhanced connection is analyzed through parametric and numerical investigations, with a particular focus on its behavior under fire. The results indicate that all types of ConXL connections maintain stable hysteresis curves, even at elevated temperatures of up to 600 °C. These connections achieve rotations exceeding 0.04 radians without forming plastic hinges, confirming their suitability for use in special moment frames. Additionally, the incorporation of the T-stub significantly enhances the performance of the ConXL connection, especially under high-temperature conditions. Comparative analysis revealed that the T-stub increased the connections' ultimate strength by factors of 1.08, 1.11, 1.10, and 1.87 at temperatures of 20, 200, 400, and 600 °C, respectively. Predictive equations for the behavior of the enhanced system are proposed, offering a practical tool for structural design and analysis practitioners.

Citation: Thongchom C, Ghamari A, Rios AJ, Karimi I. 2025. Assessment of the performance of a novel T-Stub-enhanced ConXL moment connection under fire. *Emergency Management Science and Technology* 5: e023 https://doi.org/10.48130/emst-0025-0021

Introduction

Box columns are frequently used as components of special moment-resisting frames (SMRF) in regions with a high seismic risk. These sections are typically fabricated from four welded plates. Their large bending capacity about any axis makes these sections more efficient than wide flange sections in flexural and compression members such as beam columns[1]. Additionally, the closed shape of box columns provides high torsional stiffness, which decreases the need for lateral bracing and mitigates the strength reduction typically caused by column rotation[2]. The high ductility, energy dissipation, and post-buckling strength of box sections further enhance their suitability for use as columns of seismic moment-resisting frames. Box columns also optimize material utilization and minimize the costs associated with painting and surface maintenance through their efficient design[3]. Goswami and Murty[4] introduced an improved I-beam configuration of a box column connection to overcome the drawbacks of the flow path of discontinuous forces observed in seismic steel moment frames. Their results indicated that the mobilization of the nominal beam's plastic moment capacity with sufficient strain hardening of the beam flanges could be achieved in I-beam–box column connections. Although their concept addressed the major problem of the flow path of discontinuity forces, it was not practical or economically viable. Similarly, Ghobadi et al.[5] demonstrated the promising performance of box column connections with side stiffeners, though their practical fabrication remained a challenge. Full-scale experimental tests and finite element (FE) analyses reported in[6,7] showed that connections with adequate stiffeners, designed according to fundamental seismic principles, provided sufficient strength, stiffness, and rotational capacity. Additional research by Choi et al.[8] and Yang[9] has further advanced the understanding of box columns and their connections.

Despite the abovementioned advantages, box columns present certain challenges compared with other cross-sections. For instance, accessing the interior of box columns for welding and connecting the continuity plates is challenging, complicating welding inspections and increasing production costs. Furthermore, the presence of two parallel webs in box columns results in different behaviors in comparison with other wide-flange columns. These challenges have led to extensive research into box column connections, aiming to develop cost-effective solutions while ensuring appropriate seismic performance. One notable outcome of those efforts was the introduction of the ConXL connection in the ANSI/AISC 358-10 standard[10] as a prequalified moment connection. Figures 1 and 2 illustrate the ConXL connection.

The ConXL connection has attracted significant attention as a standardized, cost-effective, special moment biaxial connection for building applications. This connection incorporates wide-flange beams, concrete-filled square Hollow Structural Section (HSS) or built-up columns, high-strength bolts, a collar flange assembly, and a collar corner assembly. It has been prequalified and codified by the American Institute of Steel Construction (AISC). Numerical studies by Rezaeian et al.[11] and Shahidi et al.[12] examined the cyclic behavior of the ConXL connection without concrete filling in the column. Their results revealed that the seismic behavior of ConXL connections is appropriate, with no significant local buckling observed in the columns.

The seismic performance of metallic beam–column connections is usually validated through experimental and numerical studies[13,14].

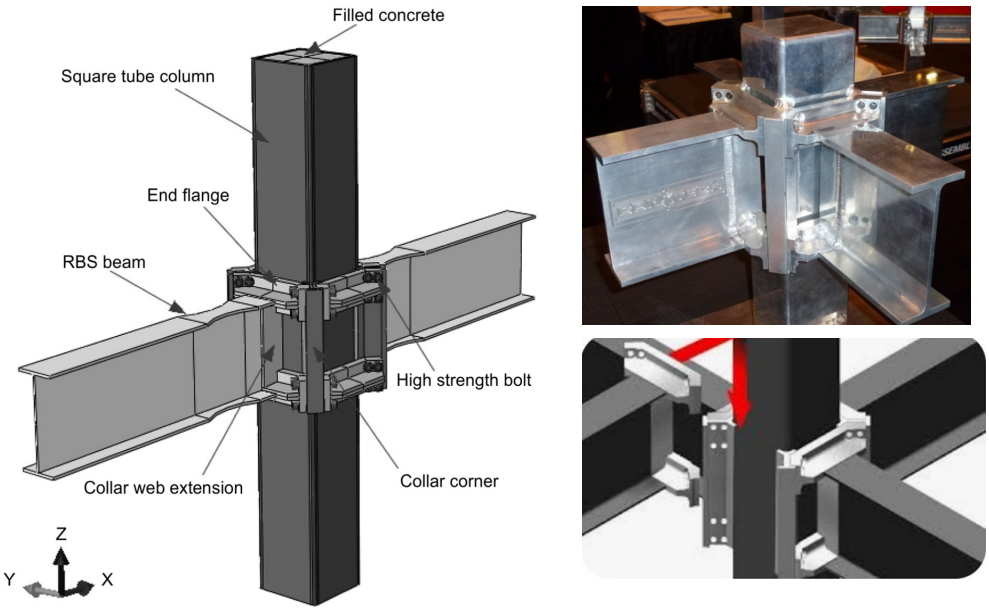

Fig. 1 Details of the ConXL connection with concrete infill, based on AISC 358-10[10]. Figure constructed by the authors.

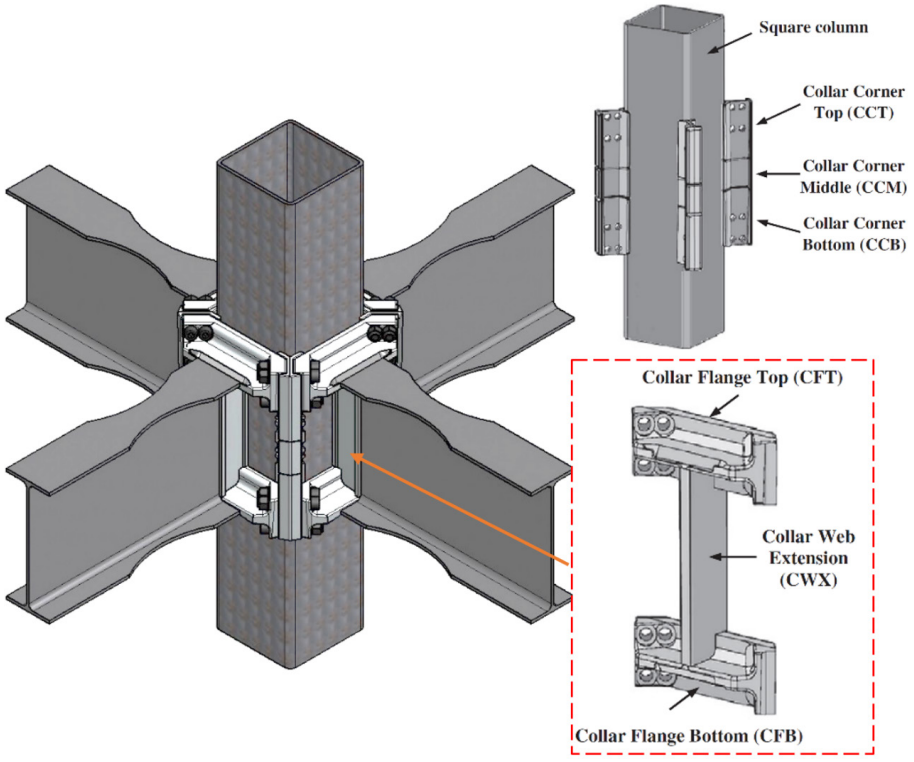

Fig. 2 Box column with ConXL connections, showing the details of the attached collar corner assemblies. Figure created by the authors.

The ConXL connection effectively addresses the issue of global bucking in box column sections. Extensive research on box columns and their connections has contributed to this achievement. Tsai et al.[15] identified that conventional connections in box columns are susceptible to damage, prompting the development of new connection designs with side stiffeners. Their experimental results demonstrated stable hysteresis loops with no degradation in strength or stiffness for the proposed connection. Similarly, Mirghaderi and Mahmoud[16] confirmed that the panel zone in box column connections exhibited yielding, influencing the overall behavior of the system. This finding highlighted the necessity of strengthening such connections, when designed in compliance with seismic design codes. The results reported in[17] highlight that failure modes such as the columns' hinge mechanism remain common under strong seismic events, despite the regulation of bending moment by various seismic codes in different countries. Furthermore, a study of the Wenchuan Earthquake (China, 2008) underscored the significance of bidirectional seismic action as a key factor contributing to failures of the columns' hinge mechanism[18].

Most studies on the seismic performance of beam–column connections conducted on three-dimensional (3D) beam–column connections have focused on concrete structures[19–21], composite

structures[22–24], or prestressed reinforced concrete structures[25–27]. However, a few relevant studies on steel beam–column connections have also been reported[28,29]. The results indicated that in beam–column joints, the effects of biaxial loading cannot be ignored in the analysis and design of spaced ductile moment-resisting frames. Green et al.[30] conducted a bidirectional load test study of a spaced semi-rigid steel beam–column joint with a floor; however, they did not show any contrast with a unidirectional loading test. Wang et al.[31] conducted a bidirectional test on a steel beam with circular tubular column connections with an outer diaphragm and found that bidirectional loading may reduce the connection strength in the decoupled loading plane but increase the connection strength and ductility in the coupled loading plane.

Fire and post-fire scenarios significantly influence the structural response of steel frames, primarily by degrading material properties such as strength, stiffness, and ductility as a result of elevated temperatures. These effects can result in reduced load-carrying capacity, increased deformation, and potential failure of critical connections, ultimately undermining their seismic response capacity. Although extensive research has been conducted on the fire performance of standard steel frame connections[32,33], there is a notable gap in the literature concerning the behavior of ConXL connections under fire and post-fire conditions. Despite their widespread use and robust performance in seismic applications, the lack of studies analyzing their structural response in these scenarios underscores the need for comprehensive investigations to ensure their safety and reliability under extreme thermal conditions.

A review of studies conducted on ConXL connections confirms their robust performance under seismic actions. The design details of these connections are included in regulations such as ANSI/AISC 341-22[34] for seismic design and ANSI/AISC 358-22[35], where the ConXL connection is prequalified for special and intermediate steel moment frames for seismic applications. Despite the demonstrated performance of the ConXL connection under seismic conditions, its behavior under fire has not yet been comprehensively investigated. Thus, its behavior under fire remains unknown, and completing a comprehensive study is required. Additionally, no prior studies have addressed the effects of variable temperatures on ConXL connections. This paper seeks to address this gap in the literature through a comprehensive numerical investigation of the behavior of ConXL connections under fire.

Materials and methods

Parametric study

FE models were used to analyze the performance of the ConXL connection. Figure 3 illustrates the details of the different ConXL connection models' configurations studied here. As shown in this figure, three types of ConXL were examined. For each model, a name was designed that consisted of four parts. The first part, C, represents the ConXL. The second letter is related to the reduced beam section (RBS), which indicates the model with (R) or without (NR) an RBS. The third letter represents the T-stub, where T and NT are used for models with and without a T-stub, respectively. Two numbers as two parts are used at the end of name to represent the thickness of the columns and the temperature applied to the model. First, the model C-NR-NT was created according to the ANSI/AISC 341-22 standards[34]. Then a RBS was incorporated in the beam to create the C-R-NT model. Finally, a T-stub was added to the ConXL as a proposed idea to improve the connection, thus resulting in the C-NR-T model.

The beam and columns (width: 24 mm × 68 mm; cross-section: 406 mm × 406 mm) with thicknesses of 12 and 20 mm, respectively,

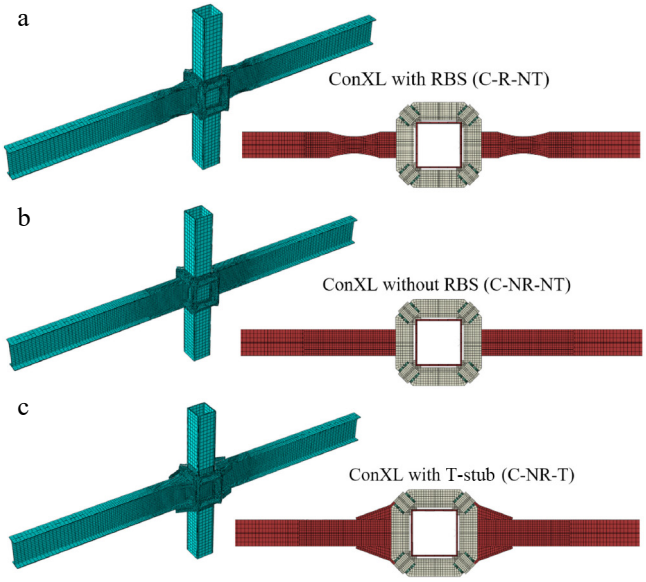

Fig. 3 Types of ConXL connections considered in the parametric study: (a) ConXL with an RBS (the C-R-NT model); (b) ConXL without an RBS (C-NR-NT model); and (c) ConXL with a T-stub (C-NR-T model).

were used for the simulation. The connection was designed according to the AISC/ANSI 358-22 standards[35]. First, the models were analyzed under cyclic loading (T_u = 20 °C). Then, to consider the behavior of the model, different temperatures, $T_u = i$, were applied and the models were analyzed under cyclic loading. For this consideration, the temperatures of T_u = 200, 400, and 600 °C were adopted.

According to ANSI/AISC 358-22[35], the beam and connections were designed, based on the computed probable maximum moment at the plastic hinge, M_{pr}, as presented in Eq. (1):

$$M_{pr} = C_{pr} R_y F_y Z_e \quad (1)$$

where, F_y is the specified minimum yield stress of the yielding element; Z_e is the effective plastic section modulus of the section at the location of the plastic hinge; R_y represents the ratio of the material ultimate stress, F_u, to the expected material yield stress, F_y; and C_{pr} is computed as $(F_y + F_u) / (2F_y)$. In addition, the shear force at each plastic hinge location, V_h, is determined from a free-body diagram of the portion of the beam between the plastic hinge locations, L_h. This calculation assumes that the moment at the center of the plastic hinge is M_{pr} and the gravity load, $V_{gravity}$, acting on the beams between plastic hinges, is as presented in Equation (2):

$$V_h = \frac{M_{pr}}{L_h} + V_{gravity} \quad (2)$$

Finite element models and simulation technique

In this paper, to simulate the FE models, ABAQUS software was used. To simulate all parts of the models, the C3D8R solid element was used. This solid element is an eight-node brick element containing a reduced integration aspect with hourglass control. The tangential behavior with a friction coefficient of 0.4 was used for the contact of the bolts. Normal behavior with hard contact was used for other elements that were touching. For meshing the elements, standard structural meshing with hexahedral mesh was utilized. Accordingly, the mesh size was 2–20 mm for different elements. For the beam, in the predicted location of plastic hinge formation, a smaller mesh size was used than that in the beam length outside the area of plastic hinge formation. A very small mesh size was applied for the bolts and other components with short lengths. Figure 4 illustrates the schematic view of the model with the selected mesh sizes.

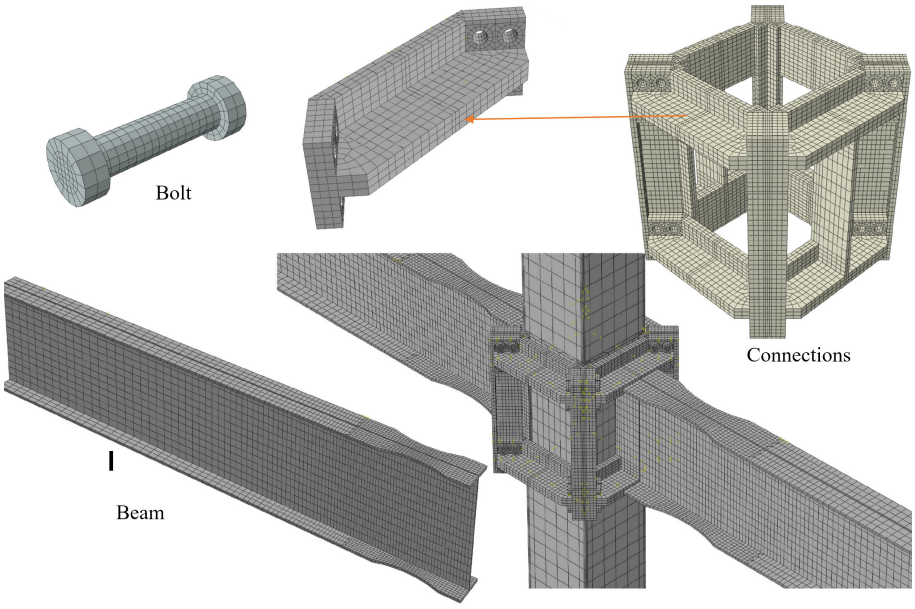

Fig. 4 A schematic view of the FE model, showing the meshing.

Boundary conditions and materials

In this paper, each system comprising two beams as a planar state are considered, as shown in Fig. 5. According to ANSI/AISC 358-22[35], the acceptable rotation of connection is 0.04 rad. Therefore, lateral loads are applied to the columns to achieve an inter-story drift of 5% to consider the connection with a rotation of 0.04 rad and to understand the system's behavior under rotation greater than the limitations of ANSI/AISC 358-22[35].

To simplify the moment frame, it is assumed that the height and length of the frame are equal to 3,500 and 7,768 mm, respectively. The lateral loading is applied to the model as shown in Fig. 6, according to the ANSI/AISC 358-22[35] specifications. A36 steel was used for the beams and columns with a yield stress (F_y), ultimate stress (F_u), and modulus of elasticity equal to 240 MPa, 370 MPa, and 200 GPa, respectively. On the basis of ASTMA574[36], the bolts were modeled using F_y = 1,050 MPa and F_u = 1,150 MPa. Finally, for the collar system, material properties of F_y = 390 MPa and F_u = 510 MPa were used according to ASTM A572 Gr50.

As an alternative, time–temperature curves from International Organization for Standardization (ISO) 834[37], and EN 1991: 1-2[38] (the Eurocode parametric fire curve) can be used to consider the effects of fire. As shown in Fig. 7, ISO curves only have a heating phase. These curves are commonly used for furnace-based testing and are not influenced by ventilation or other factors that would affect an actual fire. Accordingly, the ISO 834 standard[37] was used in this paper. In contrast, Eurocode parametric curves include a cooling phase and vary depending on the thermal inertia of the enclosure (b), the opening factor (O), and the fire's loading density ($q_{t,d}$).

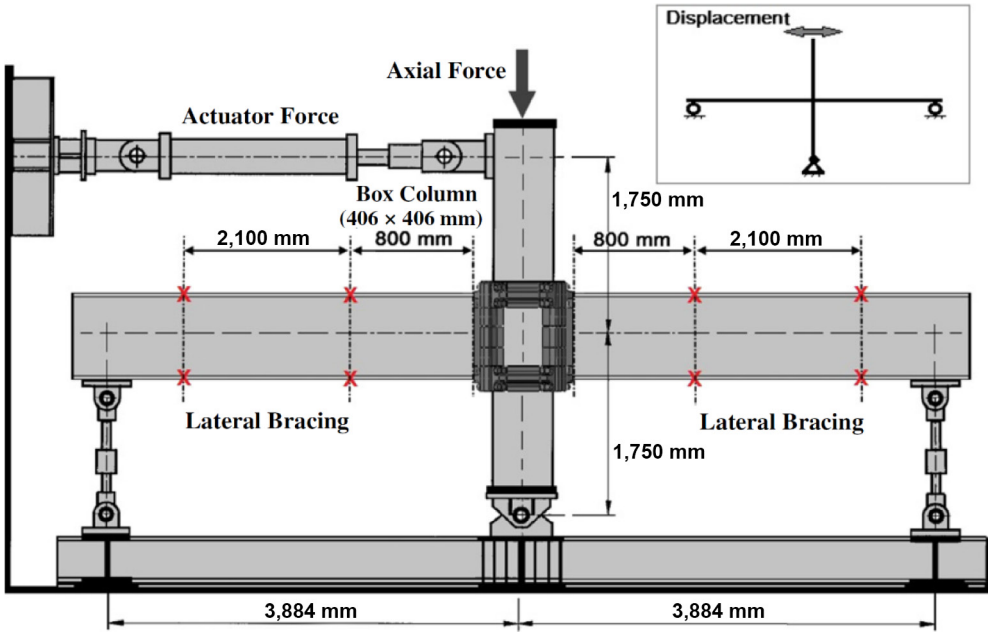

Fig. 5 Boundary conditions adopted for calibration of the initial FE model.

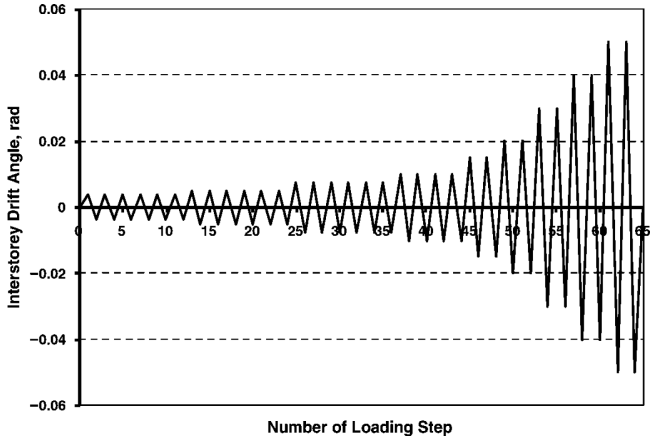

Fig. 6 Cyclic loading diagram based on ANSI/AISC 358-22[35].

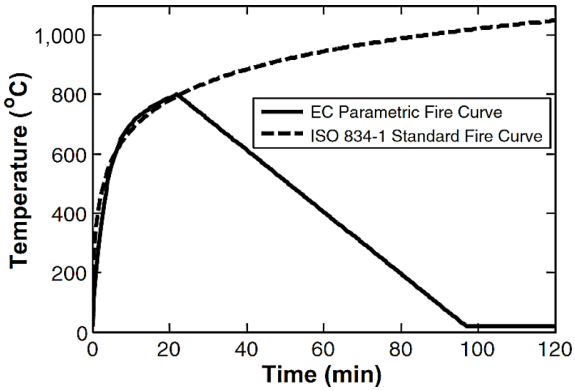

Fig. 7 The ISO standard fire curve and EC parametric fire curve applied to the FE models.

Varying these parameters affects the peak fire temperature, the fire's duration, and rate of heating and cooling. This cooling phase is important, as it results in thermal contraction, which can produce large tensile forces that cause connections to fail[39,40].

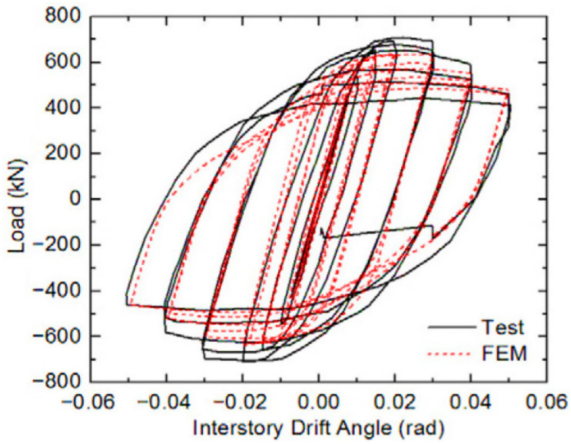

Fig. 8 Comparing the test results presented in ConXtech[41] against the FE simulation's results.

Calibration and verification of the FE model

To calibrate and verify the FE numerical model, an experimental test reported in[41] was selected and simulated using ABAQUS. Accordingly, the test results and FE results are compared in Fig. 8. As can be observed in this figure, the two hysteretic curves are in good agreement. By achieving an acceptable error (less than 10% to calculate the ultimate strength) in this model, other FE models will be considered with confidence (because of the acceptable error) in the accuracy of the results.

Results and discussion

Hysteresis curves

In Fig. 9, the hysteresis curves of the C-NR-T, C-NR-NT, and C-R-NT FE models are compared for the different temperature values

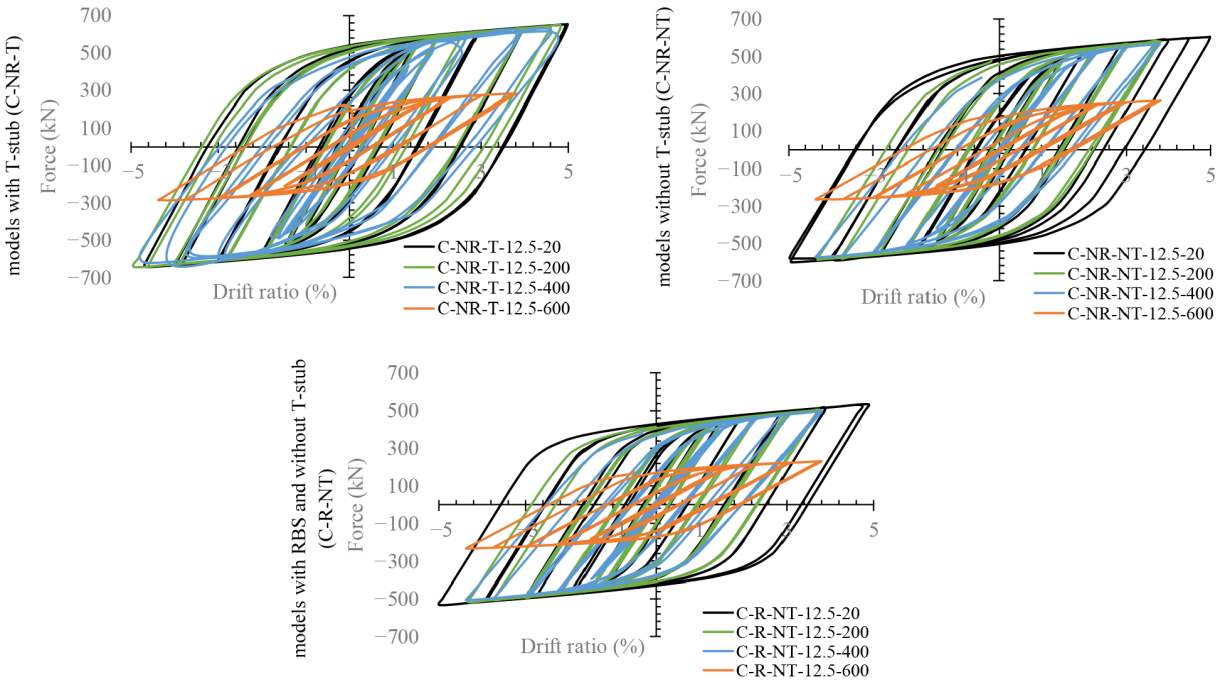

Fig. 9 Comparing the results considering the effects of fire.

considered. As shown in this figure, as expected, fire affects the response of the models. The rate of reduction is different from the rate of the increase in temperature. At T_u < 400 °C, no considerable reduction is seen in the hysteresis curves. Moreover, by increasing the temperature from ambient temperature to 400 °C, the rate of reduction in hysteresis is much lower than the one observed for T_u = 600 °C. Accordingly, the rate of reduction and the effect of the variable on the response of the models are investigated in the next subsections. RBS (C-R-NT) connections cause a lower ultimate strength than the other types of connection at all temperatures.

Yielding scenarios

The von Misses stresses of the ConXL connection components are shown in Fig. 10 to consider the yielding and hinge formation over the elements. To simplify the discussion of the results, only the elements at ambient temperature and at T_u = 600 °C are shown. As illustrated in Fig. 10, for all types of elements, hinges form at the two ends of the beams, as expected, to produce desirable performance. The collar under ambient temperature for all types of connection remains elastic, which confirms the suitable behavior of the ConXL. For the conventional ConXL with and without an RBS, yielding emerges on the panel zone of the columns, but the column can carry the load. A suitable hinge forms on the proposed ConXL, where the hinge is formed at the end of T-stub, which is far from the columns and collar. Moreover, no yielding occurred on the columns at T_u = 600 °C, and all types of connections show acceptable performance. Although the connection has been designed for ambient temperatures, negligible yielding occurs at the collar system around the bolts. However, all bolts managed to yield but were not ruptured. The T-stub made the system have the yield as in ambient system, which is considerable.

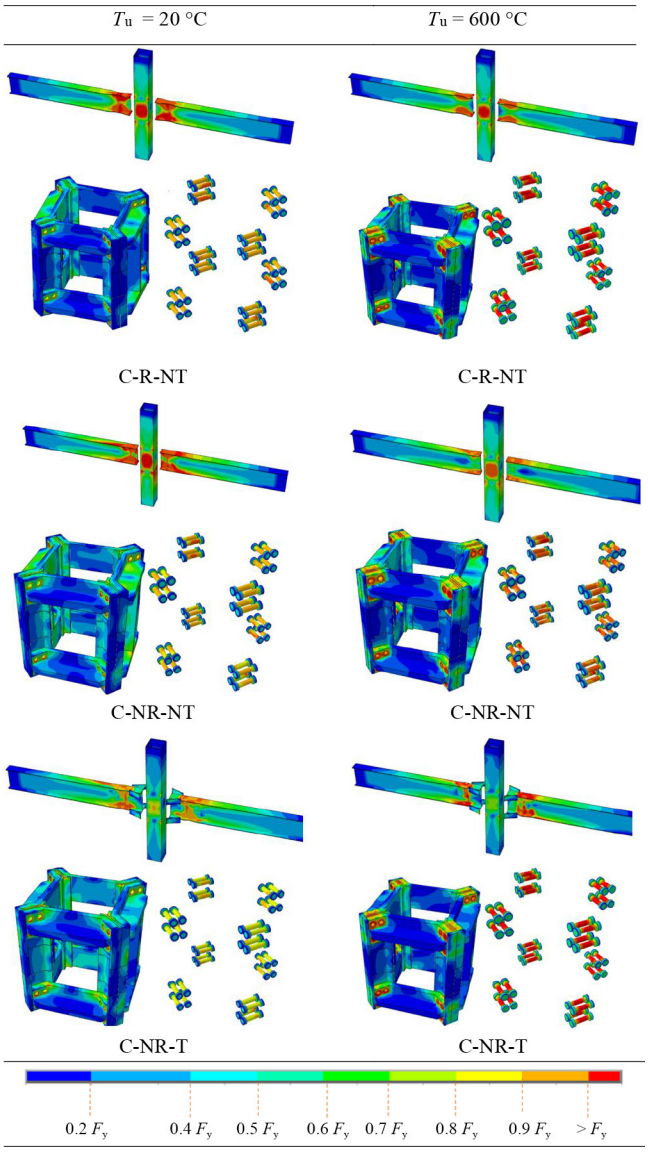

Fig. 10 The hinge formation of the elements.

The effect of the T-stub on the hysteresis curves of the system

Figure 11 illustrates the hysteresis curves of the C-NR-NT and C-NR-T models at different temperatures. As revealed in this figure, all models present a stable hysteresis curve with no degradation in strength and stiffness, and no pinching in the curves. For all specimens, for rotations more than 0.04 rad, the moment is more than 80% of the plastic moment of the beam (M_{pb}). As shown, although there is no filler concrete or continuity plates in all specimens, they all have acceptable seismic behavior and seismic post-fire behavior under cyclic loading. Comparing the models with and without a T-stub indicates that the T-stub improves the hysteresis curve of the ConXL connection. The connections with the T-stub show a greater rotation capacity than the conventional ConXL. The connection with higher rotation capacity has higher ductility and stability. In addition, adding the T-stub improved the hysteresis. This represents an improvement in the strength and energy dissipation, as will be discussed in the following subsections.

Ultimate strength

In Table 1, the ultimate strength of the FE models is listed. The results revealed that by increasing T_u, the capacity of the system is reduced, but the rate of reduction for the conventional ConXL (with and without RBS) and yjr proposed ConXL are different. When the T_u rises from the ambient temperature to 400 °C, the ultimate strength is reduced by 7%, 6%, and 4%, respectively, for the conventional ConXL with and without an RBS and the proposed ConXL. The noticeable finding is that the T-stub has a considerable effect in the T_u = 600 °C scenario. At this temperature, the reduction in the ultimate strength of the conventional ConXL (with and without an RBS) is around 56%, but with a T-stub, it improved by 24%. Moreover, a comparison of the results of the conventional ConXL (without an RBS) and the proposed ConXL indicates that the T-stub causes an increase in the ultimate strength of the system by 1.08, 1.11, 1.10, and 1.87 times for T_u = 20, 200, 400, and 600 °C, respectively. Therefore, the T-stub has a considerable effect on the strength of the system, especially at higher temperatures. Comparing the

Table 1. Comparing the ultimate strength of the models.

Models	P_u (kN)	M (kN·m)	$\frac{M_{T_u=i}}{M_{T_u=20\,°C}}$	$\frac{E_{Model\ with\ T}}{E_{Model\ without\ T}}$	$\frac{E_{Model\ with\ RBS}}{E_{Model\ without\ RBS}}$
C-NR-T-12.5-20	652.33	1,141.6	1.00	1.08	
C-NR-T-12.5-200	643.00	1,125.3	0.99	1.11	
C-NR-T-12.5-400	623.23	1,090.7	0.96	1.10	
C-NR-T-12.5-600	495.59	867.28	0.76	1.87	
C-NR-NT-12.5-20	605.45	1,059.5	1.00		
C-NR-NT-12.5-200	580.70	1,016.2	0.96		
C-NR-NT-12.5-400	568.60	995.05	0.94		
C-NR-NT-12.5-600	264.79	463.38	0.44		
C-R-NT-12.5-20	534.29	935	1.00		0.88
C-R-NT-12.5-200	506.37	886.15	0.95		0.87
C-R-NT-12.5-400	497.95	871.42	0.93		0.88
C-R-NT-12.5-600	231.32	404.81	0.43		0.87

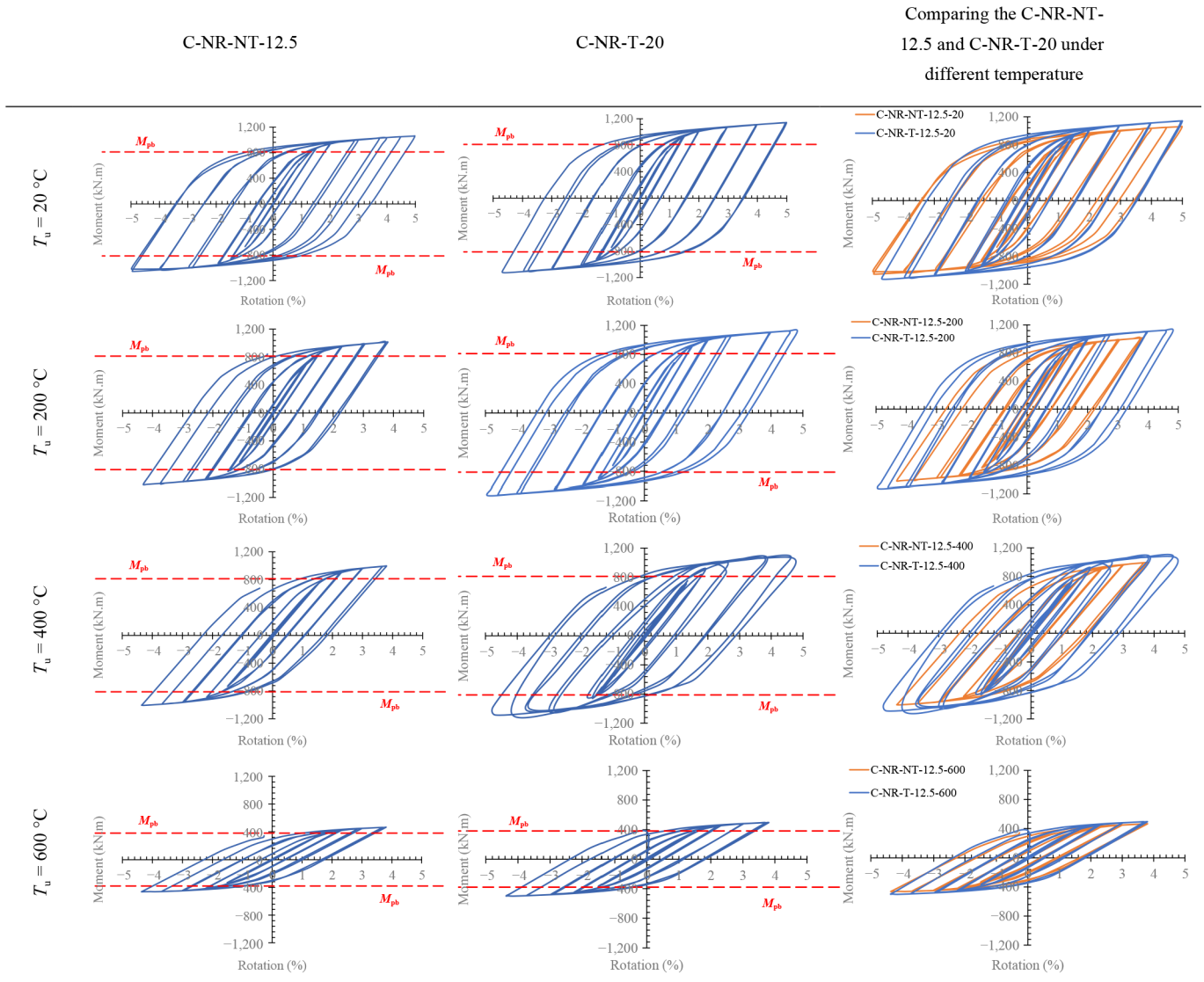

Fig. 11 ConXL connection hysteresis curves comparing the models.

conventional ConXL with and without an RBS reveals that with the RBS, the ultimate strength is reduced by around 12% for all temperatures. Therefore, the RBS has a constant effect on the connection for all temperatures. Referring to Fig. 11, it can be observed that the moment capacity of all connections studied remains practically constant under 400 °C and suffers a linear drop in capacity between temperature ranges of 400–600 °C. To predict the behavior of the system with the ConXL connection, Equations (3), (4), and (5) are proposed. These equations help structural designers to create a primary design and to predict the post-fire performance of the system.

Stiffness

As expected, by increasing the applied loading as well as the temperature, the stiffness of any structures tends to be reduced. The stiffness *K* of the FE models is listed in Table 2. At all temperatures applied, the T-stub causes a 13% increase in *K*, and the RBS connection causes a 4% decrease in the system's *K*. The results show that the presence of a T-stub or RBS connection has the same trend at all temperatures. Moreover, the presence of a T-stub or RBS showed the same decreasing trend with increasing temperatures. Referring to Table 2, it can be seen that by increasing the temperature from the ambient temperature to 200, 400, and 600 °C, the *K* of all models decreases by around 10%, 30%, and 70%, respectively. It confirms that the rate of reduction up to 400 °C is lower than that at temperatures greater than 400 °C.

Comparing the results confirms that the reduction in elastic stiffness is strongly affected by temperature changes rather than type of

Table 2. Comparing the elastic stiffness of the models.

Models	*K* (kN/mm)	$\frac{K_{T_u=i}}{K_{T_u=20\,°C}}$	$\frac{E_{Model\ with\ T}}{E_{Model\ without\ T}}$	$\frac{E_{Model\ with\ RBS}}{E_{Model\ without\ RBS}}$
C-NR-T-12.5-20	13,256	1.00	1.12	
C-NR-T-12.5-200	12,034	0.91	1.13	
C-NR-T-12.5-400	9,337.8	0.70	1.13	
C-NR-T-12.5-600	4,102.0	0.31	1.13	
C-NR-NT-12.5-20	11,850	1.00		
C-NR-NT-12.5-200	10,621	0.90		
C-NR-NT-12.5-400	8,266.5	0.70		
C-NR-NT-12.5-600	3,630.5	0.31		
C-R-NT-12.5-20	11,435	1.00		0.96
C-R-NT-12.5-200	10,246	0.90		0.96
C-R-NT-12.5-400	7,972.8	0.70		0.96
C-R-NT-12.5-600	3,498.1	0.31		0.96

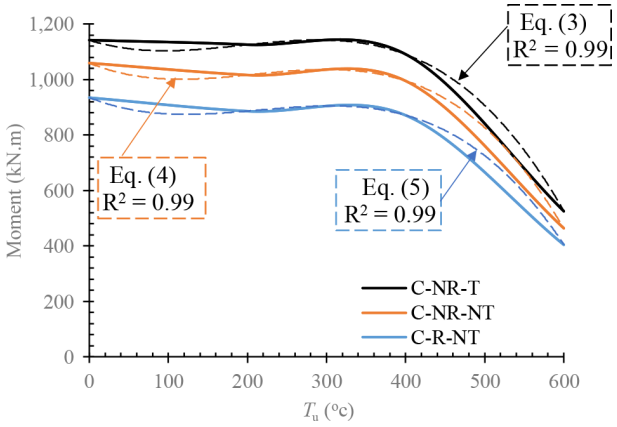

Fig. 12 Proposed equations to predict the capacity of the C-NR-T, C-NR-NT, and C-R-NT models.

connection. For this reason, in Fig. 12, the *K* of the models is plotted versus the applied temperature.

The proposed equations, Eqs. (3) to (5), have been based on the results of the paper and are useful for primary design. Subsequently, after determining the configuration and predicting the behavior of the structure, suitable analysis is required.

$$M = -0.00005\,T_u^3 + 0.0062\,T_u^2 - 0.89\,T_u + 1141 \quad \text{ConXL (with T-stub, without RBS)} \tag{3}$$

$$M = -0.00005\,T_u^3 + 0.0069\,T_u^2 - 1.16\,T_u + 1059 \quad \text{ConXL (with T-stub, without RBS)} \tag{4}$$

$$M = -0.00005\,T_u^3 + 0.0065\,T_u^2 - 1.14\,T_u + 935 \quad \text{ConXL (with T-stub, without RBS)} \tag{5}$$

As shown in Fig. 13, the rate of the reduction in stiffness is dissimilar at different temperatures. Generally, the downward and decreasing process of stiffness with a T-stub starts earlier than that of the conventional ConXL. At ambient temperatures, both the

Table 3. Comparing the energy dissipation of the models.

Models	*E* (kN·m)	$\frac{E_{T_u=i}}{E_{T_u=20\,°C}}$	$\frac{E_{Model\ with\ T}}{E_{Model\ without\ T}}$	$\frac{E_{Model\ with\ RBS}}{E_{Model\ without\ RBS}}$
C-NR-T-12.5-20	270.78	1.00	1.10	
C-NR-T-12.5-200	234.42	0.87	1.39	
C-NR-T-12.5-400	213.99	0.79	1.60	
C-NR-T-12.5-600	69.20	0.26	1.13	
C-NR-NT-12.5-20	245.25	1.00		
C-NR-NT-12.5-200	169.14	0.69		
C-NR-NT-12.5-400	134.14	0.55		
C-NR-NT-12.5-600	61.37	0.25		
C-R-NT-12.5-20	215.51	1.00		0.88
C-R-NT-12.5-200	157.23	0.73		0.93
C-R-NT-12.5-400	134.18	0.62		1.00
C-R-NT-12.5-600	60.78	0.28		0.99

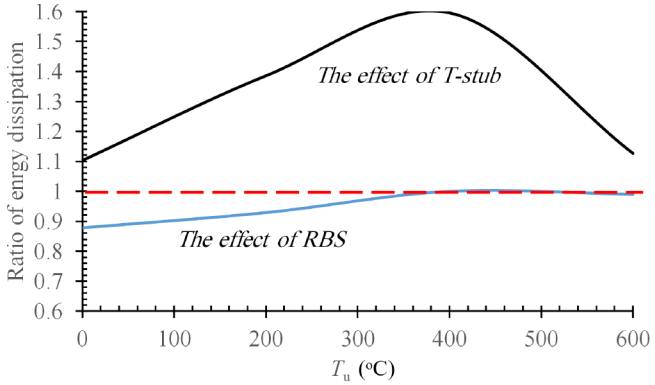

Fig. 14 Comparing the energy dissipation capacity of the models in the different temperature scenarios explored.

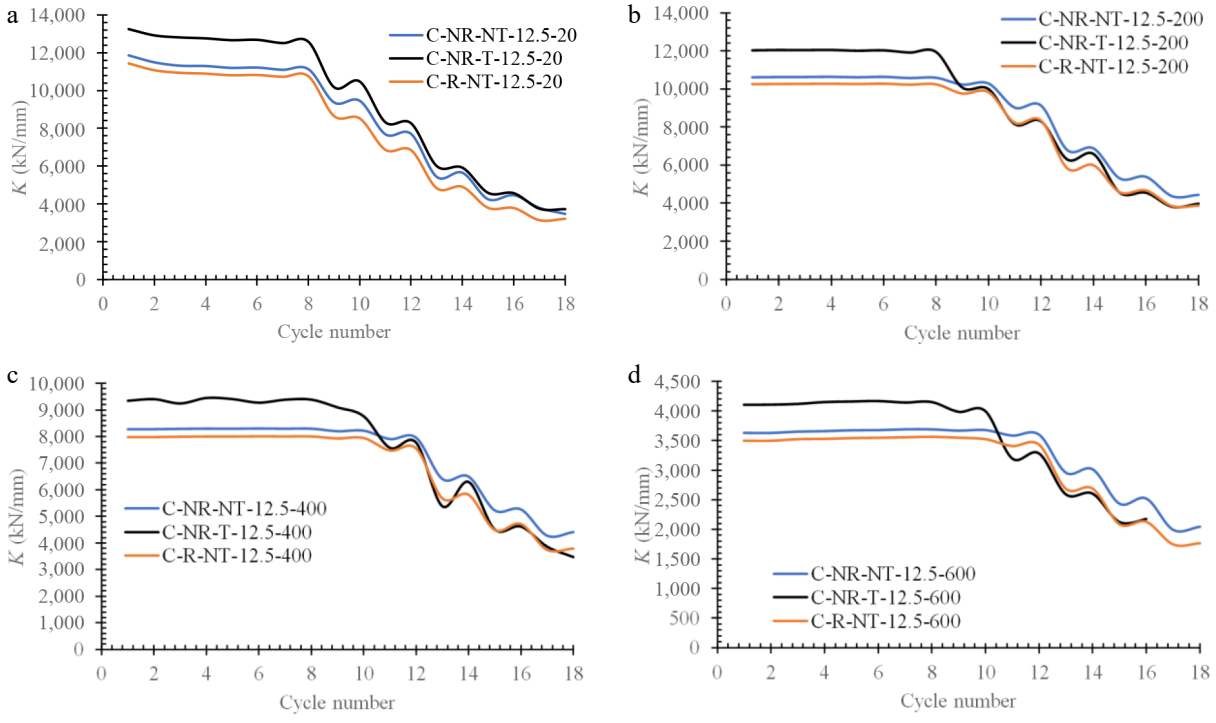

Fig. 13 Comparing the elastic stiffness of the C-NR-NT-12.5, C-NR-T-12.5, and C-R-NT-12.5 models at (a) T_u = 0 °C, (b) T_u =200 °C, (c) T_u = 400 °C, and (d) T_u = 600 °C.

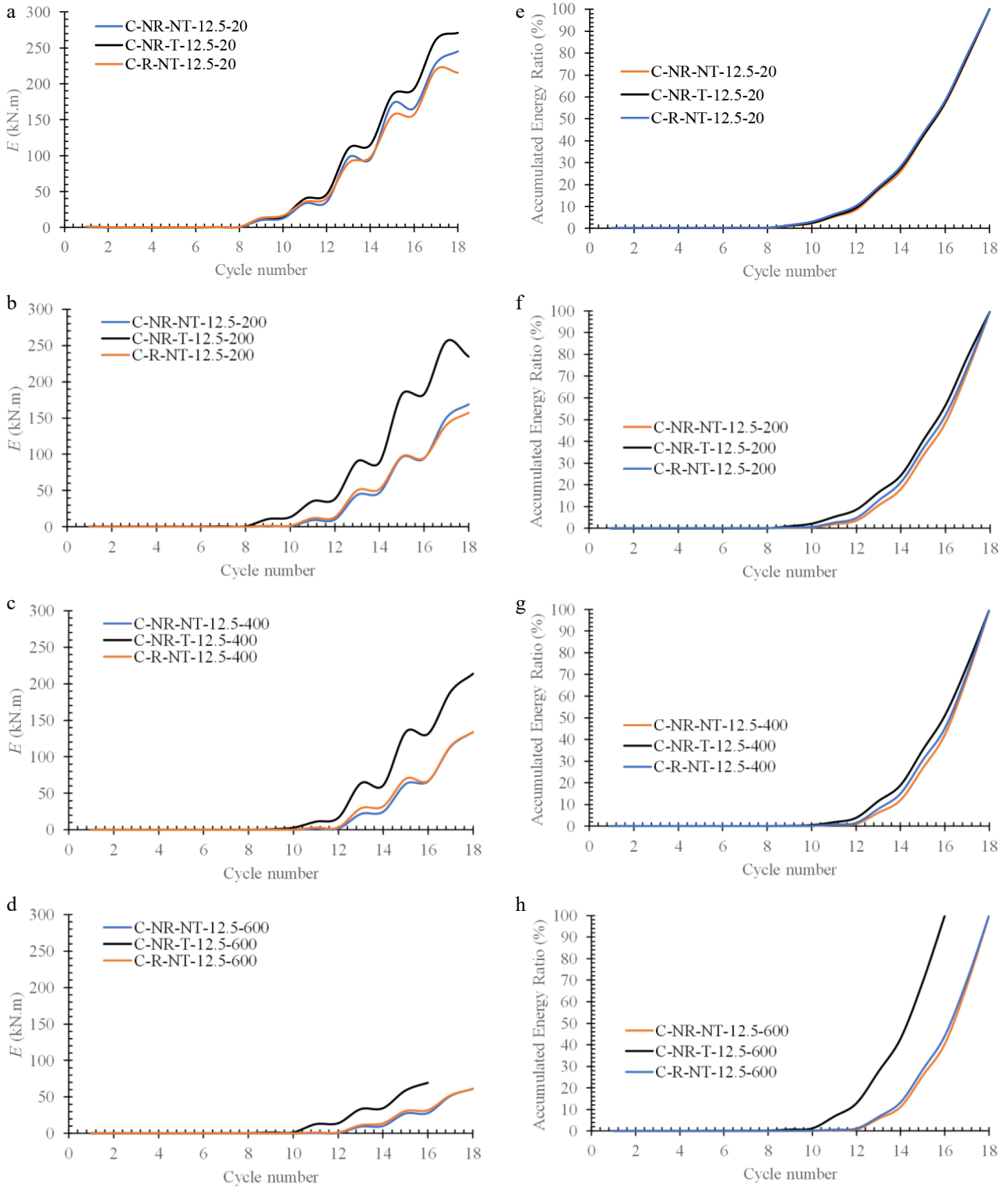

Fig. 15 Comparing the energy dissipation of the C-NR-NT-12.5, C-NR-T-12.5, and C-R-NT-12.5 models at (a) T_u = 20 °C, (b) T_u =20 °C, (c) T_u = 400 °C, (d) T_u = 600 °Cand the accumulated energy ratio of the C-NR-NT-12.5, C-NR-T-12.5, and C-R-NT-12.5 models at (e) T_u = 0 °C, (f) T_u = 200 °C, (g) T_u = 400 °C, (h) T_u = 600 °C.

conventional ConXL and the ConXl with a T-stub show a reduction in their rotation by 1.5%. At T_u = 200 °C and T_u > 200 °C, this range is 1.5% and 2% for the conventional ConXL and 2% and 3% for the ConXL with a T-stub, respectively. Although the ConXL with a T-stub has a greater stiffness than the conventional ConXL, it tends to reduce sooner than the conventional ConXL.

Energy dissipation

The energy dissipation *E* of the analyzed models is listed in Table 3. Comparing the results listed in Table 3 indicated that the T-stub provides an enhancement in the energy dissipation *E* of the connections. With the T-stub, *E* improves by 10%–60%, which is significant. This finding is plotted in Fig. 14, where the vertical axis represents

the ratio of the *E* of the compared models to the *E* of the C-NR-NT model. A noticeable finding is that an RBS affects the *E* of the system under ambient temperatures and has a negligible impact on the *E* of the system at high temperatures.

In Fig. 15, the energy dissipation of the models versus the cycle number is plotted. According to the figure, the rate of *E* is dissimilar at different temperatures, whereas the ConXL connections with and without an RBS have a similar rate. At ambient temperatures, both the conventional ConXL and the ConXl with a T-stub initially have an energy dissipation of 1.5%, which coincides with the reduction in stiffness. Correspondingly, at T_u = 200 °C and T_u > 200 °C, this range is 1.5% and 2% for the conventional ConXL and the ConXL with a T-stub, and 2% and 3%, respectively.

Conclusions

This paper investigated the behavior of the ConXL connection, including an innovative enhancement to improve its seismic and performance under fire after seismic loading was applied, using parametric and numerical analyses.

(1) Although ConXL connections at ambient tempratures, with or without an RBS and with a T-stub, showed stable performance without a loss of stiffness or strength, even unfilled with concrete. At 600 °C, they exceeded 0.04 radians of rotational capacity without plastic hinges, meeting AISC's special moment frame standards.

(2) The temperature affects the response of the connections. At 400 °C, strength dropped by 7%, 6%, and 4% for the conventional ConXL with an RBS, that without an RBS, and the T-stub-enhanced ConXL, respectively. At 600 °C, the conventional ConXL lost ~56% of its strength, whereas the T-stub-enhanced system lost 24%.

(3) The T-stub-enhanced ConXL connection demonstrates superior performance under heat, particularly in its energy dissipation characteristics. At room temperature, both the conventional and T-stub-enhanced connections started dissipating energy at the same degree of rotation (1.5%).

(4) As temperatures rose above 200 °C, the T-stub-enhanced connection required a higher rotation (3%) to start dissipating energy compared with the conventional one (2%). This indicates that the enhanced connection is more robust and maintains its stiffness for longer under elevated temperatures, highlighting its advantage for practical high-temperature applications.

(5) To complete and expand the recent study, it is recommended to consider the T-stub's economical aspects in comparison with other models under ambient and high temperatures.

Author contributions

The authors confirm their contributions to the paper as follows: conceptualization, visualization, supervision and funding acquisition: Thongchom C, Ghamari A; methodology, data curation and writing – original draft preparation: Ghamari A; software and formal analysis: Karimi I; validation and investigation: Thongchom C, Ghamari A, Rios AJ; resources and project administration: Thongchom C; writing – review and editing: Thongchom C, Rios AJ. All authors reviewed the results and approved the final version of the manuscript.

Data availability

The original contributions presented in this study are included in the article/supplementary material. Further inquiries can be directed to the corresponding author.

Acknowledgments

This research is supported by the Thailand Science Research and Innovation (TSRI) Fundamental Fund for fiscal year 2026.

Conflict of interest

The authors declare that they have no conflict of interest.

Dates

Received 20 August 2025; Revised 2 December 2025; Accepted 10 December 2025; Published online 29 December 2025

References

1. Sophianopoulos SD, Deri AE. 2000. *State of the Art Report on Connection Performance* (FEMA-355D). Washington DC: World Journal of Mechanics www.nehrp.gov/pdf/fema355d.pdf
2. Sherman DR. 1996. Designing with structural tubing. *Engineering Journal* 33:101–9
3. Mirghaderi SR, Torabian S, Keshavarzi F. 2010. I-beam to box–column connection by a vertical plate passing through the column. *Engineering Structures* 32:2034–48
4. Goswami R, Murty CVR. 2008. Improved configuration of I-beam to box column connections in seismic steel moment frames. *Proceedings of the 14th World Conference on Earthquake Engineering, Beijing, China, 12–17 October, 2008*. Analytical Chemistry www.iitk.ac.in/nicee/wcee/article/14_05-05-0011.PDF
5. Ghobadi MS, Ghassemieh M, Mazroi A, Abolmaali A. 2009. Seismic performance of ductile welded connections using T-stiffener. *Journal of Constructional Steel Research* 65:766–75
6. Lee SL, Ting LC, Shanmugam NE. 1993. Use of external T-stiffeners in box-column to I-beam connections. *Journal of Constructional Steel Research* 26:77–98
7. Ting LC, Shanmugam NE, Lee SL. 1993. Design of I-beam to box-column connections stiffened externally. *Engineering Journal* 30:141–49
8. Choi SM, Park SH, Yun YS, Kim JH. 2010. A study on the seismic performance of concrete-filled square steel tube column-to-beam connections reinforced with asymmetric lower diaphragms. *Journal of Constructional Steel Research* 66:962–70
9. Yang C, Yang JF, Su MZ, Liu CZ. 2016. Numerical study on seismic behaviours of ConXL biaxial moment connection. *Journal of Constructional Steel Research* 121:185–201
10. The AISC Board of Directors. 2010. *ANSI/AISC 358-10 Prequalified Connections for Special and Intermediate Steel Moment Frames for Seismic Applications*. 2010. Chicago: American Institute of Steel Construction (AISC) www.aisc.org/products/publication/historic-standards/prequalified-connections/prequalified-connections-for-special-and-intermediate-steel-moment-frames-ansiaisc-358-10/
11. Rezaeian A, Jamal-Omidi M, Shahidi F. 2014. Seismic behavior of ConXL rigid connection in box-columns not filled with concrete. *Journal of Constructional Steel Research* 97:79–104
12. Shahidi F, Rezaeian A, Jamal-Omidi M, Shahidi F. 2015. Investigation of the ConXL moment connection cyclic behavior in box columns without filling concrete with different arrangement of collar bolts. *The Structural Design of Tall and Special Buildings* 24:317–50
13. Moncayo-Matute FP, Chicaiza-Machuca DF, Vélez-Sisalima IS, Torres-Jara PB, Vázquez-Silva E. 2024. Seismic behavior of flange-web welded plate connections in tubular and concrete-filled columns using finite element analysis. *Applied Sciences* 14:6494
14. Ramirez Ortiz C, Areiza Palma G, Gutierrez Amador A, Ramirez Duque J, Cano Buitron R, et al. 2022. Seismic behavior of a steel beam-to-concrete-filled steel tubular column connection using external diaphragms. *Applied Sciences* 12:3618
15. Tsai, KC, Lin KC, Liu MC. 1992. Seismic behavior of steel beam-t-box column connections. *Proceedings of the 10th World Conference on Earth-*

quake Engineering, Madrid, Spain, 19–24 July, 1992. Rotterdam: A.A. Balkema. pp. 2903–9 www.iitk.ac.in/nicee/wcee/article/10_vol5_2903.pdf
16. Mirghaderi R. Mahmoud M. 2006. Seismic behaviour of panel zones in beam to column connections with non-planner webs in moment resisting steel frames. *Proceedings of the 4th International Conference on Earthquake Engineering, Taipei, Taiwan, 12–13 October, 2006*. Taipei, Taiwan, China: National Center for Research on Earthquake Engineering (NCREE). pp. 1545–52 www.researchgate.net/publication/242136975
17. Comité Euro-International du Béton. 1998. *Seismic design of reinforced concrete structures for controlled inelastic response: design concepts*. Leeds, UK: Emerald Publishing Limited. doi: 10.1680/sdorcsfcir.26414
18. Wang Y. 2008. Lessons learned from the "5.12" Wenchuan earthquake: evaluation of earthquake performance objectives and the importance of seismic conceptual design principles. *Earthquake Engineering and Engineering Vibration* 7:255–62
19. Leon R, Jirsa JO. 1986. Bidirectional loading of R.C. beam-column joints. *Earthquake Spectra* 2:537–64
20. Akguzel U, Pampanin S. 2010. Effects of variation of axial load and bidirectional loading on seismic performance of GFRP retrofitted reinforced concrete exterior beam-column joints. *Journal of Composites for Construction* 14:94–104
21. Zheng Q, Chen S, Lin W. 2024. Numerical study on seismic performance of a new prefabricated reinforced concrete structural system integrated with recoverable energy-dissipating RC walls. *Buildings* 14:3243
22. Kawaguchi J, Morino S, Sugimoto T. 1996. Elasto-Plastic Behavior of Concrete-Filled Steel Tubular Frames. *Proceeding of an Engineering Foundation Conference, New York, USA, 2–7 June, 1996*. New York, USA: American Society of Civil Engineers (ASCE). pp. 272–81 www.researchgate.net/publication/37672090
23. Fan JS, Zhou H, Nie JG, Li QW. 2012. Research on seismic responses of 3D joints with CFT column and composite beam under bi-directional loading. *Journal of Building Structures* 33:50–58 (in Chinese)
24. Li W, Yang Y, Kong Z, Huang W, Wang Y, et al. 2024. Cyclic performance and environmental impact of precast demountable RCS joints. *Buildings* 14:3071
25. Li L, Mander JB, Dhakal RP. 2008. Bidirectional cyclic loading experiment on a 3D beam–column joint designed for damage avoidance. *Journal of Structural Engineering* 134:1733–42
26. Amaris A, Pampanin S, Palermo A. 2006. Uni and bi-directional quasi static tests on alternative hybrid precast beam column joint subassemblies. *Proceedings of the New Zealand Society of Earthquake Engineering 2006 Conference (NZSEE 2006), Napier, New Zealand, 10–12 March, 2006*. Napier, New Zealand: University of Canterbury. Civil Engineering. pp. 1–8 https://ir.canterbury.ac.nz/items/e4706d80-1b03-4f05-893e-7c419bacb6ee
27. Pekgokgoz RK, Yakut I. 2024. Investigation of passive controlled post-tensioning system on the structural behaviour of precast reinforced concrete beam–column connections. *Buildings* 14:3910
28. Gemechu TD, Lu L. 2024. Analysis of factors affecting the seismic performance of widened flange connections in mid-flange H-beams and box columns. *Buildings* 14:3170
29. Gallegos M, Nuñez E, Herrera R. 2020. Numerical study on cyclic response of end-plate biaxial moment connection in box columns. *Metals* 10:523
30. Green TP, Leon RT, Rassati GA. 2004. Bidirectional tests on partially restrained, composite beam-to-column connections. *Journal of Structural Engineering* 130:320–27
31. Wang W, Chen Y, Li W, Leon RT. 2011. Bidirectional seismic performance of steel beam to circular tubular column connections with outer diaphragm. *Earthquake Engineering & Structural Dynamics* 40:1063–81
32. Wang W, Lyu X, Zheng J, Yi S, Li J, et al. 2024. Post-fire seismic performance of concrete-filled steel tube frame structures considering soil-structure interaction (SSI). *Buildings* 14:555
33. Dehcheshmeh EM, Rashed P, Broujerdian V, Shakouri A, Aslani F. 2023. Predicting seismic collapse safety of post-fire steel moment frames. *Buildings* 13:1091
34. The Committee on Specifications. 2022. *Seismic Provisions for Structural Steel Buildings* (ANSI/AISC 341-22). Chicago, IL, USA: American Institute of Steel Construction (AISC) 546 pp. www.aisc.org/Seismic-Provisions-for-Structural-Steel-Buildings-ANSIAISC-341-22-Download
35. The Connection Prequalification Review Panel. 2022. *Prequalified Connections for Special and Intermediate Steel Moment Frames for Seismic Applications* (ANSI/AISC 358-22). Chicago, IL, USA: American Institute of Steel Construction (AISC). 358 pp. www.aisc.org/products/publication/standards/aisc-358/prequalified-connections-for-special-and-intermediate-steel-moment-frames-for-seismic-applications/
36. ASTM International. 2021. *Standard Specification for Alloy Steel Socket-Head Cap Screws* (ASTM A574-21). West Conshohocken, PA, USA: ASTM International. pp. 1–7 doi: 10.1520/A0574-21
37. International Organization for Standardization (ISO). 2014. *Fire resistance tests—Elements of building construction—Part 11: Specific requirements for the assessment of fire protection to structural steel elements* (ISO 834-11:2014). Geneva, Switzerland: International Organization for Standardization (ISO). pp. 1–53 www.iso.org/standard/57595.html
38. European Commission. 2002. *Eurocode 1: Actions on structures—Part 1-2: General actions—Actions on structu res exposed to fire* (EN 1991-1-2:2002). Brussels, Belgium: European Committee for Standardization (CEN). pp. 1–63 https://eurocodes.jrc.ec.europa.eu/EN-Eurocodes/eurocode-1-actions-structures
39. Franssen JM, Vila Real P. 2016. *Fire Design of Steel Structures: EC1: Actions on structures—Part 1-2: Actions on structure exposed to fire; EC3: Design of steel structures—Part 1-2: Structural fire design*. 2nd Edition. Chichester, UK: John Wiley & Sons, Ltd. pp. 1–450 doi: 10.1002/9783433607008
40. Rasoulnia A, Broujerdian V, Ghamari A. 2024. An improved flexural design procedure of steel plate I-girders considering elastic lateral torsional buckling at elevated temperatures. *The Structural Design of Tall and Special Buildings* 33:e2171
41. ConXtech. 2022. *The Structural Steel Building System That is Simply Better for Institutional Projects* (Technical Brochure). Pleasanton, CA, USA: ConXtech. https://www.conxtech.com/wp-content/uploads/2022/11/Conxtech-Education-Experience.pdf